Journal of Engineering Mathematics **41:** 329–344, 2001.

On the thermal field of a separating wall jet

P. G. DANIELS[1] and J. T. RATNANATHER[2]
[1]*Department of Mathematics, City University, Northampton Square, London EC1V 0HB, UK*
[2]*Center for Imaging Science and Center for Computational Medicine and Biology, Johns Hopkins University, Baltimore, MD 21218, USA*

Received 29 March 2000; accepted in revised form 18 May 2001

Abstract. Thermal wall jets are found in a variety of applications in geophysics, mammalian physiology and electronics, to name but a few. The thermal field of a separating wall jet is studied for a range of values of the Prandtl number of the fluid. The structure of the jet near the point of separation is described by a free interaction in which the fundamental problem is to solve the boundary-layer equations in a viscous sublayer close to the wall. Analytical and numerical solutions are found for the thermal field within the sublayer for the case of a wall at a fixed temperature. In particular, the wall heat transfer is obtained and effects of upstream influence within the thermal field are discussed. The large-Prandtl-number limit is considered in detail and it is shown that the main variation of the thermal field occurs within a region in the immediate neighbourhood of the point of separation. An upstream-downstream iterative method is used to obtain a numerical solution for this thermal field.

Key words: boundary layer, convection, heat transfer, jet, separation.

1. Introduction

The asymptotic structure of a wall jet near a point of separation was considered by Smith and Duck [1]. They showed that a mutually-reinforcing interaction on a short streamwise length scale could lead to a rise in pressure and separation of the jet from the wall. Locally the flow consists of a two-tier structure, a main deck which accommodates an inviscid displacement of the jet and a viscous sublayer, or lower deck, governed by the boundary-layer equations. Within the sublayer there is a streamwise pressure gradient proportional to the curvature of the jet displacement, a relation which forms the key element of the interaction. Smith and Duck solved the lower-deck problem numerically using an approximation due to Flugge-Lotz and Reyhner [2] in which the inertial term involving the streamwise velocity gradient is set to zero in the region of reverse flow. This allows the computation to proceed beyond separation and leads to results in reasonable agreement with asymptotic predictions of the separated flow structure at large values of the downstream coordinate. In this structure the dividing streamline lies within a shear layer which diverges from the wall as the square of the downstream coordinate and encloses a slowly-moving region of reverse flow.

For a thermal wall jet the temperature field of this separated flow is also of interest. One application may be found in heat exchange systems, an example of which is the cooling of electronic circuit boards in computers [3]. Flow separation in a corner region is generally accompanied by a reduction of heat transfer which can lead to the overheating of electronic components, with disastrous consequences for the system as a whole. Another application may be found in mammalian physiology [4], [5, pp. 116–120], [6] in which flow separation in enclosures is accompanied by loss of heat transfer and may help to maintain body temperature

in extreme climates. In this paper, consideration is given to the effect of flow separation on the temperature field near separation and the consequent implications for the local heat transfer.

The basic jet flow is taken to be the free-convection boundary layer generated on a heated vertical wall by a linear thermal gradient. Such jets arise in thermally-driven cavity flows and also in geophysical flows involving thermal stratification (see, for example, [7]). Double-deck structures for these and related flows have been studied in various contexts in [8–15]. A specific application of the present analysis would arise, for example, where separation is caused by a small protrusion from the wall or a local change in heating. If the protrusion is comparable in size to the lower deck then the entire separation and reattachment of the jet can be described within the lower-deck system, as in the analysis of Ghosh Moulic and Yao [13]. Here, the more general situation is considered where the protrusion is sufficiently large to provoke separation well upstream, where the wall surface is flat. Although the jet flow ahead of separation is taken to be that associated with a heated wall in a stratified fluid, the analysis is also applicable to more general jet flows of the type described in [1].

The double-deck structure near separation is outlined in Section 2 and leads to the fundamental lower-deck problem for which the velocity field has been computed in [1]. The corresponding problem for the temperature field is also obtained and numerical solutions are presented for a range of Prandtl numbers in Section 3. Asymptotic properties of the solution are also discussed. Eigensolutions associated with upstream influence and non-uniqueness of the flow downstream of separation are identified and alternative forms of the temperature field in the separated flow far downstream of separation are discussed. Section 4 considers the structure of the thermal field for large Prandtl numbers and it is shown that the key problem is to solve the thermal boundary-layer equation in a region within the lower deck in the immediate neighbourhood of the separation point. The solution of this problem is described in Section 5 and the results are discussed in Section 6.

2. Flow structure near separation

A free-convective flow is generated on a heated vertical wall $y^* = 0$, $-\infty < x^* < \infty$ by maintaining the wall at a fixed temperature

$$T^* = T_0^* + \Delta T^*(1 + x^*/l), \tag{1}$$

where $T_0^* + \Delta T^* x^*/l$ is the temperature of the ambient fluid, l being the height over which the wall temperature rises by an amount ΔT^*. The governing equations for steady, two-dimensional Boussinesq flow may be written in the non-dimensional form

$$\frac{\partial \overline{u}}{\partial \overline{x}} + \frac{\partial \overline{v}}{\partial \overline{y}} = 0, \tag{2}$$

$$\sigma^{-1}\left(\overline{u}\frac{\partial \overline{u}}{\partial \overline{x}} + \overline{v}\frac{\partial \overline{u}}{\partial \overline{y}}\right) = -\frac{\partial \overline{p}}{\partial \overline{x}} + \nabla^2 \overline{u} + R\overline{T}, \tag{3}$$

$$\sigma^{-1}\left(\overline{u}\frac{\partial \overline{v}}{\partial \overline{x}} + \overline{v}\frac{\partial \overline{v}}{\partial \overline{y}}\right) = -\frac{\partial \overline{p}}{\partial \overline{y}} + \nabla^2 \overline{v}, \tag{4}$$

$$\overline{u}\frac{\partial \overline{T}}{\partial \overline{x}} + \overline{v}\frac{\partial \overline{T}}{\partial \overline{y}} = \nabla^2 \overline{T}, \tag{5}$$

where $T^* = T_0^* + \Delta T^* \overline{T}$, $(x^*, y^*) = l(\overline{x}, \overline{y})$ and the velocity components and pressure are made non-dimensional with respect to κ/l and $\rho\nu\kappa/l^2$, respectively, where ρ is the density. Also $\sigma = \nu/\kappa$ is the Prandtl number of the fluid, where ν is the kinematic viscosity and κ is the thermal diffusivity, and $R = \alpha g \Delta T^* l^3/\kappa\nu$ is the Rayleigh number, where α is the coefficient of thermal expansion and g is the acceleration due to gravity, which acts in the negative x^* direction.

From (1), the appropriate boundary conditions at the wall are

$$\overline{T} = 1 + \overline{x}, \qquad \overline{u} = \overline{v} = 0, \qquad \overline{y} = 0, \tag{6}$$

while at large distances

$$\overline{T} \to \overline{x}, \qquad \overline{u} \to 0, \qquad \overline{y} \to \infty. \tag{7}$$

An exact parallel-flow solution of (2–7) exists of the form (see [16], [7])

$$\overline{T} = \overline{x} + T_0(\overline{Y}), \qquad \overline{u} = R^{1/2} U_0(\overline{Y}), \qquad \overline{v} = 0, \qquad \overline{p} = \frac{1}{2} R \overline{x}^2, \tag{8}$$

where $\overline{Y} = R^{1/4}\overline{y}$ and

$$T_0 = \mathrm{e}^{-\overline{Y}/\sqrt{2}} \cos(\overline{Y}/\sqrt{2}), \qquad U_0 = \mathrm{e}^{-\overline{Y}/\sqrt{2}} \sin(\overline{Y}/\sqrt{2}). \tag{9}$$

In the limit $R \to \infty$ the flow takes the form of a boundary layer of width $\overline{y} = O(R^{-1/4})$. Although the velocity alternates in direction towards the edge of the layer the primary flow is an upward buoyancy-driven motion adjacent to the wall. It should also be noted that this flow is independent of the Prandtl number of the fluid.

Now consider the modification to this jet flow caused by a localized disturbance which may be due to a small protrusion from the wall or a local change in thermal boundary conditions. The implication of [1] is that this can lead to upstream influence within the jet and the occurrence of separation through a local interaction on a short streamwise length scale of order $R^{-3/14}$. The location of this interaction region will depend upon the precise nature of the disturbance which, it is assumed here, is sufficient to provoke separation at a distance well upstream ($>> R^{-3/14}$). Near the point of separation, the flow assumes a two-tier structure consisting of a main deck of width $\overline{y} = O(R^{-1/4})$ and a viscous sublayer, or lower deck, of width $\overline{y} = O(R^{-9/28})$. A local streamwise variable $\tilde{x}$ is defined by

$$\overline{x} = \overline{x}_0 + R^{-3/14}\tilde{x}, \tag{10}$$

where $\overline{x} = \overline{x}_0$ is the point of separation and the main-deck solution is given by

$$\begin{aligned} \overline{u} &= R^{1/2} U_0(\overline{Y}) + R^{3/7} U_1 + \cdots, & \overline{p} &= \tfrac{1}{2} R \overline{x}_0^2 + R^{6/7} P_1 + \cdots, \\ \overline{v} &= R^{11/28} V_1 + \cdots, & \overline{T} &= \overline{x}_0 + T_0(\overline{Y}) + R^{-1/14} T_1 + \cdots, \end{aligned} \tag{11}$$

where substitution in (2–5) gives

$$U_1 = \tilde{A}(\tilde{x}) U_0', \quad V_1 = -\tilde{A}'(\tilde{x}) U_0, \quad T_1 = \tilde{A}(\tilde{x}) T_0' \tag{12}$$

and

$$P_1 = \sigma^{-1} \tilde{A}''(\tilde{x}) \int_0^{\overline{Y}} U_0^2(y')\, \mathrm{d}Y' + \tilde{p}(\tilde{x}). \tag{13}$$

Here $\tilde{A}(\tilde{x})$ and $\tilde{p}(\tilde{x})$ are functions of $\tilde{x}$ to be determined.

In the lower deck

$$\begin{aligned} \overline{u} &= R^{3/7}\tilde{u}(\tilde{x},\tilde{y})+\cdots, \qquad \overline{p} = \tfrac{1}{2}R\overline{x}_0^2 + R^{6/7}\tilde{p}(\tilde{x})+\cdots, \\ \overline{v} &= R^{9/28}\tilde{v}(\tilde{x},\tilde{y})+\cdots, \qquad \overline{T} = \overline{x}_0 + 1 + R^{-1/14}\tilde{T}(\tilde{x},\tilde{y})+\cdots, \end{aligned} \tag{14}$$

where $\overline{y} = R^{-9/28}\tilde{y}$. Matching with the main-deck solution requires

$$\tilde{u} \sim U_0'(0)(\tilde{y}+\tilde{A}(\tilde{x})), \qquad \tilde{T} \sim T_0'(0)(\tilde{y}+\tilde{A}(\tilde{x})), \qquad \tilde{y}\to\infty \tag{15}$$

and from (13), application of Bernoulli's equation at the edge of the jet requires,

$$\tilde{p}(\tilde{x}) = -\sigma^{-1}\tilde{A}''\int_0^\infty U_0^2(Y')\,\mathrm{d}Y'. \tag{16}$$

It is convenient to introduce the scale transformations

$$\begin{aligned} &\tilde{x} = \lambda^{-5/7}\gamma^{3/7}\sigma^{-1/7}x, \qquad \tilde{y} = \lambda^{-4/7}\gamma^{1/7}\sigma^{2/7}y, \\ &\tilde{u} = \lambda^{3/7}\gamma^{1/7}\sigma^{2/7}u, \qquad \tilde{v} = \lambda^{4/7}\gamma^{-1/7}\sigma^{5/7}v, \\ &\tilde{p} = \lambda^{6/7}\gamma^{2/7}\sigma^{-3/7}p, \qquad \tilde{T} = \lambda^{-4/7}\gamma^{1/7}\sigma^{2/7}\mu T, \qquad \tilde{A} = \lambda^{-4/7}\gamma^{1/7}\sigma^{2/7}A, \end{aligned} \tag{17}$$

where $\lambda = U_0'(0) = 1/\sqrt{2}$, $\mu = T_0'(0) = -1/\sqrt{2}$ and $\gamma = \int_0^\infty U_0^2(Y')\,\mathrm{d}Y' = 1/4\sqrt{2}$, and then the lower-deck problem is to solve

$$\frac{\partial u}{\partial x} + \frac{\partial v}{\partial y} = 0, \tag{18}$$

$$u\frac{\partial u}{\partial x} + v\frac{\partial u}{\partial y} = -\frac{\mathrm{d}p}{\mathrm{d}x} + \frac{\partial^2 u}{\partial y^2}, \tag{19}$$

$$u\frac{\partial T}{\partial x} + v\frac{\partial T}{\partial y} = \sigma^{-1}\frac{\partial^2 T}{\partial y^2} \tag{20}$$

subject to

$$u = v = T = 0, \qquad y = 0, \tag{21}$$

$$u \sim y + A(x), \qquad T \sim y + A(x), \qquad y\to\infty, \tag{22}$$

where

$$p = -\frac{\mathrm{d}^2 A}{\mathrm{d}x^2}. \tag{23}$$

Upstream, the solution must match with the undisturbed jet flow, requiring that

$$u\to y,\ T\to y,\ A\to 0,\ p\to 0, \qquad x\to-\infty. \tag{24}$$

One consequence of the rescaling (17) is that the velocity and pressure fields u, v, p are independent of Prandtl number and are determined independently of the temperature field in the manner described in [1]. The temperature field T must then be found by solving the thermal boundary-layer equation (20) for specified values of the Prandtl number.

From (19) and (24), the stream function ψ of the lower-deck flow defined by

$$u = \frac{\partial \psi}{\partial y}, \qquad v = -\frac{\partial \psi}{\partial x} \tag{25}$$

has the behaviour

$$\psi \sim \tfrac{1}{2}(y + A)^2 + p + O(\exp), \qquad y \to \infty \tag{26}$$

and it is of interest to note from (20) that the temperature field contains terms which decay algebraically, with

$$T \sim y + A + p(y + A)^{-1} + O(y^{-3}), \qquad y \to \infty. \tag{27}$$

3. Finite Prandtl numbers

Numerical solutions of the lower-deck problem (18–24) were computed for a wide range of Prandtl numbers using a finite difference marching procedure based on the Keller-box method. Results were obtained using a FLARE approximation [2] in which the terms $u\partial u/\partial x$ in the momentum equation and $u\partial T/\partial x$ in the temperature equation are neglected wherever $u < 0$. The velocity field is independent of Prandtl number and is computed from a suitable initial station $x = x_{-\infty}$ by applying a small positive increment to the pressure. This is sufficient to initiate the mutually reinforcing interaction which, as the computation proceeds downstream leads to separation and growth of the pressure p to a plateau value $p_0 \approx 1{\cdot}22$ consistent with the results of [1]. The origin of coordinates $x = 0$, $y = 0$ is chosen to correspond to the point of separation.

As $x \to \infty$, the dividing streamline which emanates from the point of separation is located within a shear layer where $\xi = (y + A(x))/x^{1/3} = O(1)$ and

$$\psi \sim x^{2/3} G_0(\xi), \quad x \to \infty, \tag{28}$$

with

$$\begin{aligned} &G_0''' + \tfrac{2}{3} G_0 G_0'' - \tfrac{1}{3} G_0'^2 = 0, \\ &G_0 \sim \tfrac{1}{2}\xi^2 + 0, \xi \to \infty, \\ &G_0' \to 0, \xi \to -\infty. \end{aligned} \tag{29}$$

The boundary conditions follow from matching with the forward flow outside the shear layer, where ψ is given by (26), and from the fact that there is no significant flow between the shear layer and the wall. The solution obtained originally in [17] has the property $G_0(-\infty) = -\alpha_0 = -1{\cdot}257$. The corresponding pressure and displacement fields are

$$p \sim p_0 + p_1 x^{-8/3}, \quad A \sim -\frac{1}{2} p_0 x^2, \quad x \to \infty, \tag{30}$$

so that the dividing streamline departs from the wall as the square of the distance downstream of separation. Between the shear layer and the wall there is an inviscid-dominated region of weak reverse flow where

$$\psi \sim -(-2p_1)^{1/2} y/x^{4/3}, \qquad x \to \infty \ (0 < y/x^2 < \frac{1}{2} p_0). \tag{31}$$

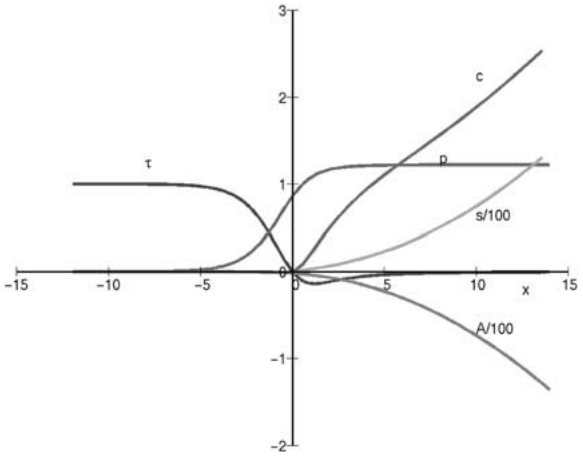

Figure 1. Pressure $p(x)$, displacement $A(x)$ and skin friction $\tau(x) = \partial u/\partial y(x, y = 0)$ for the lower-deck free interaction as obtained in [1]. The curves giving the location $y = s(x)$ of the dividing streamline $\psi = 0$ and the streamwise velocity $u = c(x)$ along the dividing streamline are also shown.

The pressure correction p_1 is determined by matching with the shear layer as $p_1 = -2\alpha_0^2/p_0^2$ and also drives the upstream flow in a wall layer of thickness $y = O(x^{7/6})$ where $\psi = O(x^{-1/6})$. Details are given in [1].

The computations of the velocity and pressure fields shown in Figure 1 were carried out with step lengths $\Delta x = 0{\cdot}1$, $\Delta y = 0{\cdot}1$, an outer boundary at $y = y_\infty = 140$ and a tolerance of 10^{-8} in the Newton iteration used to solve the discretized system of nonlinear equations at each downstream step; computations were initiated at $x = -11{\cdot}9$ and terminated at $x = 25{\cdot}9$. Checks on accuracy were made with other values of these parameters. Results for the temperature field are shown in Figure 2 where the wall heat transfer is displayed for Prandtl numbers varying from 0·01 to 10. The heat transfer falls dramatically ahead of and beyond separation, with the region of variation beyond separation becoming smaller as the Prandtl number increases and subject to a numerical instability which is discussed in detail below.

Temperature profiles for Prandtl numbers of 0·1 and 1 across the lower deck at various values of x are shown in Figure 3. Within the shear layer which forms as $x \to \infty$, it is envisaged that

$$T \sim x^{1/3} H_0(\xi), \quad x \to \infty, \tag{32}$$

where H_0 satisfies the equation

$$H_0'' + \sigma(\tfrac{2}{3} G_0 H_0' - \tfrac{1}{3} G_0' H_0) = 0, \tag{33}$$

together with the boundary condition

$$H_0' \to 1, \quad \xi \to \infty, \tag{34}$$

in order to match the outer form (27). It is readily established by one integration of (33) that the solution which is exponentially small as $\xi \to \infty$ cannot pass through a zero as ξ decreases, or reach zero as $\xi \to -\infty$, so that the two fundamental solutions for H_0 may be defined by the properties $H_{0_1}'(\infty) = 1$, $H_{0_1}(-\infty) = 0$ and $H_{0_2}(\infty) = 0$, $H_{0_2}(-\infty) = 1$. The general solution for H_0 which satisfies (34) can then be written in the form

$$H_0 = H_{0_1} + k H_{0_2}, \tag{35}$$

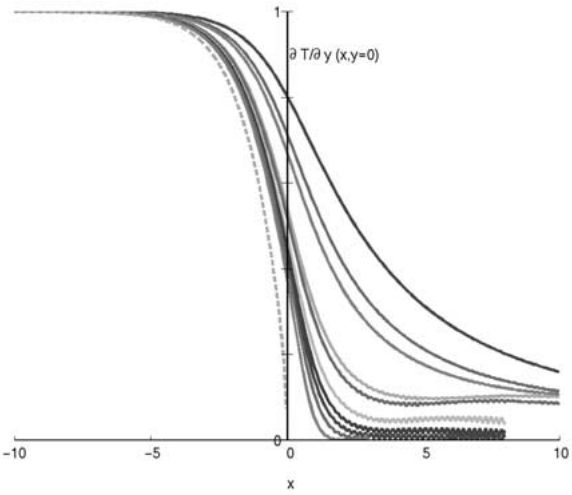

Figure 2. Wall heat transfer with Prandtl numbers 0·01, 0·05, 0·1, 0·72, 1, 2, 3, 4, 5·65, 10 increasing from right to left towards the dashed line which is the large-Prandtl-number limit: $\partial T/\partial y(x, y = 0) \sim \{\tau(x)\}^{1/2}$ (see Equation (48) below) where $\tau(x)$ is obtained from the solution in Figure 1.

where k is an arbitrary constant. The solutions H_{0_1} and H_{0_2} were computed for unit Prandtl number over the domain $-10 \leq \xi \leq 10$ and are shown, along with G_0, in Figure 4. It is interesting to note that for unit Prandtl number $H_{0_1} = G_0'$. If the constant k is non-zero it is readily shown that the inviscid reverse flow region between the shear layer and the wall is then convection-dominated, with $T \sim k(-\psi/\alpha_0)^{1/2}$ as $x \to \infty$. Such solutions may be physically realistic and indeed there may be a much wider class of solutions corresponding to the arbitrary specification of T on streamlines entering the flow field from $x = \infty$. However, in Sections 4 and 5 below, attention is focused on the possibility that $k = 0$ in which case as $x \to \infty$ there is no significant variation in T between the shear layer and the wall. This situation can be compared to the results obtained in [13] for locally separated flows produced by small protrusions on the lower-deck scale. There it was observed that the separated region acts like an insulating layer in which the heat transfer rates are reduced, the heat transfer across the almost stagnant region being mainly by conduction.

In the FLARE computations reported here, the numerical solution for T develops an oscillatory instability if x is allowed to increase too far beyond separation (see Figure 2). This is presumably connected with the neglect of upstream influence in the numerical scheme. Results for finite Prandtl numbers using an improved scheme such as that developed for the momentum equations by Saintlos *et al.* [18], [19] still need to be found, although the downstream structure of the solution, together with the possibility of a wide range of solutions corresponding to different downstream boundary conditions for T makes this a difficult task in general: see Aziz *et al.* [20] for a review of numerical schemes to solve these types of forward-backward parabolic equations. An improved scheme for the simpler problem associated with the large Prandtl number limit is described in Section 5 below, based on a method developed by Ratnanather and Daniels [21] for dealing with strongly-reversed thermal boundary-layer flows.

The manner in which upstream influence affects the temperature field beyond separation can be analysed by studying the solution near $x = 0+$. Here the stream function has the form

$$\psi = \tfrac{1}{6}ay^3 - bxy^2 + \cdots , \tag{36}$$

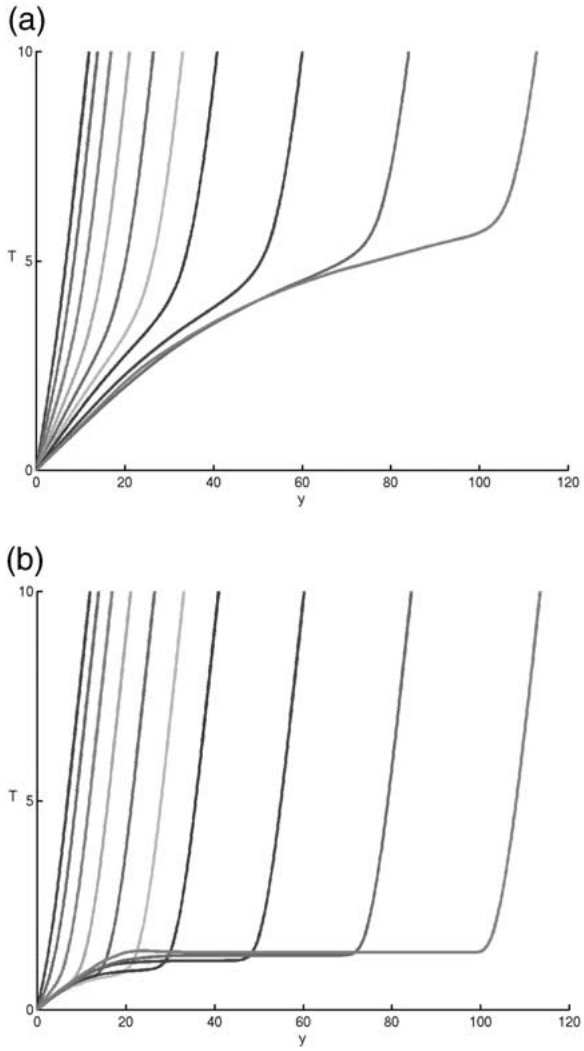

Figure 3. Temperature profiles at $x = 0{\cdot}1$, $1{\cdot}1$, $2{\cdot}1$, $3{\cdot}1$, $4{\cdot}1$, $5{\cdot}1$, $6{\cdot}1$, $8{\cdot}1$, $10{\cdot}1$, $12{\cdot}1$ (left to right) in the lower deck for (a) $\sigma = 0{\cdot}1$ and (b) $\sigma = 1$.

where $a = \mathrm{d}p/\mathrm{d}x(0) > 0$ and $b = -\frac{1}{2}\partial^2 u/\partial x \partial y(0,0) > 0$. Thus the local temperature field satisfies

$$(\tfrac{1}{2}ay^2 - 2bxy)\frac{\partial T}{\partial x} + by^2\frac{\partial T}{\partial y} = \sigma^{-1}\frac{\partial^2 T}{\partial y^2}. \tag{37}$$

Although the dominant terms in the expansion of T about the origin are regular, the most important aspect of the thermal field just beyond separation is a non-uniqueness associated with the existence of exponentially growing eigensolutions. Such solutions of (37) take the form

$$T \sim \left(\frac{xb^{4/3}\sigma^{1/3}}{a}\right)^n \exp\left\{-\frac{a^3\beta}{b^4\sigma x^3}\right\}\left(F_0(\eta) + \frac{x^3b^4\sigma}{a^3}F_1(\eta) + \cdots\right), \quad x \to 0+, \tag{38}$$

where $\eta = ay/bx$ and β is an eigenvalue to be determined. Substitution in (37) gives at leading order

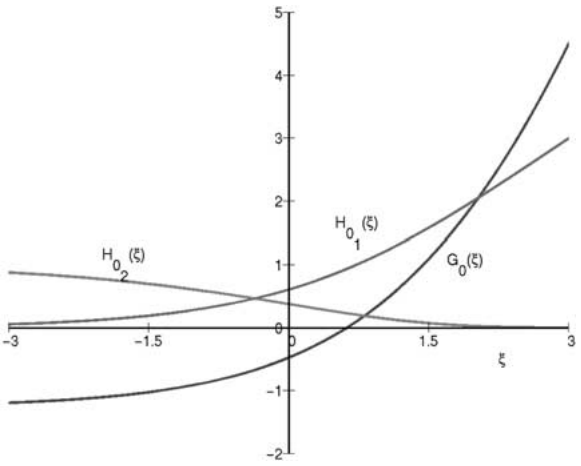

Figure 4. The fundamental solutions H_{0_1} and H_{0_2} of Equation (33) for Prandtl number $\sigma = 1$. The function G_0 is also shown.

$$F_0'' - 3\beta(\tfrac{1}{2}\eta^2 - 2\eta)F_0 = 0 \tag{39}$$

and at first order

$$F_1'' - 3\beta(\tfrac{1}{2}\eta^2 - 2\eta)F_1 = (\tfrac{1}{2}\eta^2 - 2\eta)nF_0 + (3\eta^2 - \tfrac{1}{2}\eta^3)F_0'. \tag{40}$$

Solutions of (39) which decay exponentially as $\eta \to \infty$ are of the form

$$F_0 = c_0 U(-(6\beta)^{1/2},\ (6\beta)^{1/4}(\eta - 2)), \tag{41}$$

where U is the parabolic cylinder function (see, for example, [22, p. 686]). At the wall ($\eta = 0$) it is required that $F_0 = 0$, which fixes β as a solution of

$$U(-(6\beta)^{1/2},\ -2(6\beta)^{1/4}) = 0. \tag{42}$$

This determines an infinite sequence of eigenvalues $\beta = \beta_m$, $m = 0, 1, 2, \ldots$, with

$$\beta_m^{1/2} = (m - \tfrac{1}{3})/\sqrt{6} + o(1), \quad m \to \infty. \tag{43}$$

The value of n in (38) is fixed by a consistency condition associated with the requirement that (40) has a solution which satisfies $F_1(0) = 0$ and $F_1 \to 0$ as $\eta \to \infty$. Multiplication of (39) by F_1 and (40) by F_0, subtraction and integration yields the result

$$(n + \tfrac{3}{2})(3\beta)^{-1} \int_0^\infty F_0'^2 \, \mathrm{d}\eta = 0, \tag{44}$$

from which it follows that $n = -\frac{3}{2}$. This analysis is based on (37) and therefore neglects higher-order corrections in the Taylor expansion (36) of ψ at the origin. Inclusion of such terms would lead to a more complicated expansion in (38) and quite possibly a different value of n, but the leading-order results for β and F_0 would remain unaffected. In fact the correction term involving F_1 remains valid formally in the large Prandtl number limit where (a scaled form of) Equation (37) governs the flow in a separation zone surrounding the origin (see Section 4 below). The solution (38) with $n = -\frac{3}{2}$ then applies just downstream of the separation point, as measured relative to the reduced scale of the separation zone.

The family of eigensolutions (38) allows exponentially small thermal perturbations to grow downstream of separation and prevents a reliable numerical solution from being obtained by a forward marching technique. These eigenfunctions must instead be determined from information supplied downstream of separation and are the means by which upstream influence occurs within the reverse flow region. The eigenfunctions (41) are centred around the line $\eta = 2$ which lies within the reverse flow zone $0 < \eta < 4$ just downstream of separation. They decay outwards across the line of zero streamwise velocity $\eta = 4$ and the dividing streamline $\eta = 6$, thus also influencing the thermal field in the forward-flow region where $x > 0$. The length scale x over which the eigenfunctions grow is proportional to $\sigma^{-1/3}$ so that in a numerical computation based on forward marching, breakdown can be expected to occur rapidly at large Prandtl numbers. This is observed in the FLARE computations.

It is of interest to note that upstream influence within the velocity and pressure fields can be expected to occur through eigenfunctions proportional to

$$\exp\left\{-\frac{a^3\tilde{\beta}}{b^4x^3}\right\}, \quad x \to 0+, \tag{45}$$

with the eigenvalues $\tilde{\beta}$ independent of Prandtl number. As the main purpose of the present work is to discuss the thermal field, the detailed structure of these eigensolutions will not be given here.

4. Large-Prandtl-number limit

In the limit of large Prandtl number it is clear from (20) that throughout most of the lower deck the thermal boundary layer equation is dominated by the convective terms on the left-hand side, implying that the temperature T is functionally dependent only on the stream function ψ. Upstream (as $x \to -\infty$), $\psi \to \frac{1}{2}y^2$ and $T \to y$ so that in the region $x < 0$ and outside the shear layer in $x > 0$,

$$T \sim (2\psi)^{1/2}, \quad \sigma \to \infty. \tag{46}$$

In general a thin thermal layer (where the right-hand side of (20) is significant) might be expected to occur along the wall $x < 0$. However, the solution for ψ has the behaviour $\psi \sim \frac{1}{2}y^2\tau(x)$ as $y \to 0$, where $\tau(x)$ is the skin friction shown in Figure 1. Thus the solution for T given by (46) has the linear form

$$T \sim \{\tau(x)\}^{1/2}\, y, \quad y \to 0 \ (x < 0). \tag{47}$$

Since this solution satisfies both the wall condition $T = 0$ on $y = 0$ and the full Equation (20), no adjustment to the outer solution (46) is required. The wall heat transfer in the large-Prandtl-number limit is therefore given by

$$\frac{\partial T}{\partial y}(x, y = 0) \sim \{\tau(x)\}^{1/2}, \quad x < 0, \tag{48}$$

a result which agrees with the numerical computations (see Figure 2). Note also that the outer solution (46) is consistent with the asymptotic behaviours (26) and (27) as $y \to \infty$. Result (48) expresses a simple relationship between skin friction and heat transfer; the corresponding relationship for a classical boundary layer at finite Prandtl numbers has been discussed by Lighthill [23].

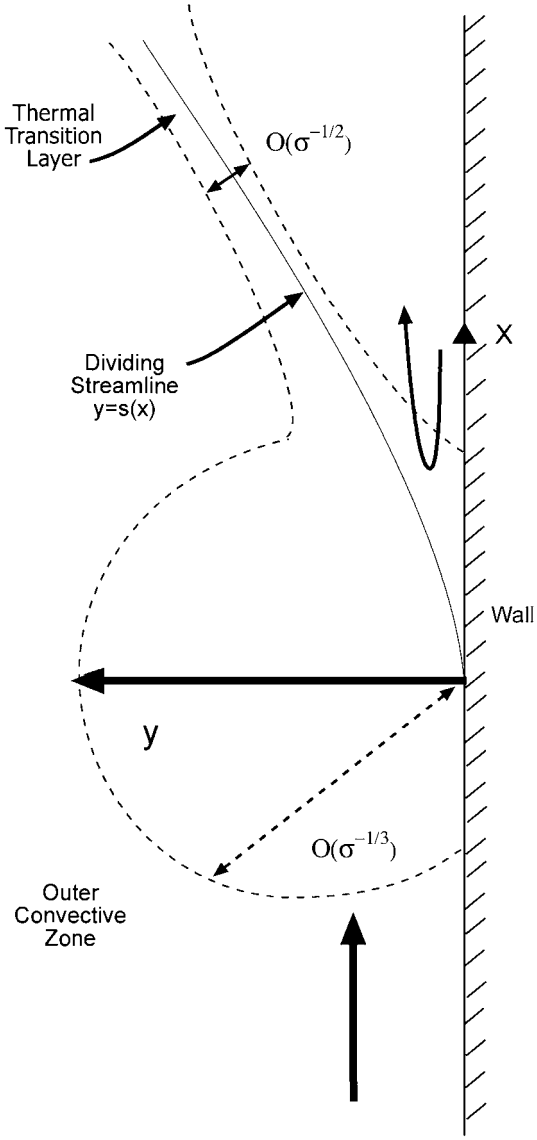

Figure 5. Schematic diagram of the lower-deck solution in the large-Prandtl-number limit.

Near the point of separation the stream function is given by (36) and the skin friction $\tau(x)$ vanishes linearly, with $\tau \sim -2bx, x \to 0$ where $b > 0$. Thus the wall heat transfer given by (48) has a square-root singularity

$$\frac{\partial T}{\partial y}(x, y = 0) \sim (2b)^{1/2}(-x)^{1/2}, \quad x \to 0-, \tag{49}$$

which must be smoothed out within a small region centred on the point of separation. In this separation zone (see Figure 5) both the convective and conductive terms must balance in (20) and on the assumption that

$$T \sim a^{1/2}b^{-1/2}\sigma^{-1/2}\theta(X, Y), \quad \sigma \to \infty, \tag{50}$$

where $x = ab^{-4/3}\sigma^{-1/3}X$, $y = b^{-1/3}\sigma^{-1/3}Y$, the function θ is found to satisfy the reduced system

$$(\tfrac{1}{2}Y^2 - 2XY)\frac{\partial\theta}{\partial X} + Y^2\frac{\partial\theta}{\partial Y} = \frac{\partial^2\theta}{\partial Y^2}, \tag{51}$$

$$\theta \sim Y(-2X)^{1/2}, \quad X \to -\infty, \tag{52}$$

$$\theta = 0, \quad Y = 0, \tag{53}$$

$$\theta \sim (\tfrac{1}{3}Y^3 - 2XY^2)^{1/2}, \quad Y \to \infty. \tag{54}$$

Locally the stream function $\psi \sim ab^{-1}\sigma^{-1}\Psi(X, Y)$ where $\Psi = \frac{1}{6}Y^3 - XY^2$ and so in the scaled variables X, Y the dividing streamline $\Psi = 0$ is the straight line $Y = 6X$; similarly, the path on which $u = 0$ is given locally by the straight line $Y = 4X$, with reverse flow occuring in the segment $Y < 4X$ for $X > 0$. This allows for upstream influence in Equation (51) and so the system must be closed by a suitable boundary condition on θ as $X \to \infty$. Near the dividing streamline the solution has the form

$$\theta \sim X^{3/4}H(\zeta), \quad X \to \infty, \tag{55}$$

where $\zeta = (Y - 6X)X^{1/2}$ and H satisfies the equation

$$H'' + 9\zeta H' - \tfrac{9}{2}H = 0 \tag{56}$$

and, from (54), the boundary condition

$$H \sim 2\sqrt{3}\zeta^{1/2}, \quad \zeta \to \infty. \tag{57}$$

If the solution between the dividing streamline and the wall is to contain only weak thermal gradients, the system for H is completed by the requirement that in the asymptotic form $H \sim K(-\zeta)^{1/2}$ as $\zeta \to -\infty$, the constant K is zero, in which case

$$H \to 0, \quad \zeta \to -\infty. \tag{58}$$

This is equivalent to the choice $k = 0$ in (35) and excludes the complementary solution for H (equivalent to H_{0_2} in (35)) given by $\exp\{-\frac{9}{4}\zeta^2\}U(1, 3\zeta)$. Thus

$$H = \sqrt{2\pi}\exp\{-\tfrac{9}{4}\zeta^2\}V(1, 3\zeta), \tag{59}$$

where V is the second parabolic cylinder function (see [22, p. 686]) and the solution for θ below the dividing streamline is then exponentially small as $X \to \infty$. A numerical solution of the system (51–54) together with the downstream behaviour corresponding to

$$K = 0 \tag{60}$$

is presented in Section 5.

The analysis of the leading-order large-Prandtl-number structure is completed by considering how the solution near the dividing streamline extends into the outer region. The position of the dividing streamline $y = s(x)$ is determined by the velocity field of [1] and from the earlier discussion has the properties $s \sim 6a^{-1}bx$, $x \to 0+$ and $s \sim \frac{1}{2}p_0x^2$, $x \to \infty$. Near this line, ψ can be approximated by $\psi \sim c(x)(y - s(x))$ where $c(x)$ is again a known function and has

the properties $c \sim 6a^{-1}b^2x^2$, $x \to 0+$ and $c \sim c_0 x^{1/3}$, $x \to \infty$, with $c_0 = G_0'(\xi_0) = 0{\cdot}934$, where $\xi_0 = 0{\cdot}620$ is the zero of G_0. The functions $s(x)$ and $c(x)$ are shown in Figure 1.

The thermal adjustment near the dividing streamline occurs in a narrow transition region (see Figure 5) where the conduction term on the right-hand side of (20) balances the convection terms, requiring a scale in y of order $\sigma^{-1/2}$. A local coordinate $\hat{y}$ is defined by writing $y = s(x) + \sigma^{-1/2}\hat{y}$ and then the solution for T is given by

$$T \sim \sigma^{-1/4}\hat{T}(x, \hat{y}), \quad \sigma \to \infty, \tag{61}$$

where $\hat{T}$ satisfies the equation

$$c(x)\frac{\partial \hat{T}}{\partial x} - c'(x)\hat{y}\frac{\partial \hat{T}}{\partial \hat{y}} = \frac{\partial^2 \hat{T}}{\partial \hat{y}^2}. \tag{62}$$

This must be solved in $x > 0$ subject to the conditions

$$\hat{T} \sim (2c(x)\hat{y})^{1/2}, \quad \hat{y} \to \infty, \tag{63}$$

$$\hat{T} \to 0, \quad \hat{y} \to -\infty \tag{64}$$

and matching with the behaviour (55) as $x \to 0$. A coordinate transformation $(x, \hat{y}) \to (\hat{x}, \hat{\psi})$ where $\hat{x}$ and $\hat{\psi}$ are defined by

$$\hat{x} = \int_0^x c(x)\,\mathrm{d}x, \quad \hat{\psi} = c(x)\hat{y}, \tag{65}$$

is now used to reduce (62–64) to the form

$$\frac{\partial \hat{T}}{\partial \hat{x}} = \frac{\partial^2 \hat{T}}{\partial \hat{\psi}^2}; \quad \hat{T} \sim (2\hat{\psi})^{1/2}, \quad \hat{\psi} \to \infty; \quad \hat{T} \to 0, \quad \hat{\psi} \to -\infty \tag{66}$$

and the relevant solution is

$$\hat{T} = \hat{x}^{1/4}\hat{H}(\hat{\zeta}), \tag{67}$$

where $\hat{\zeta} = \hat{\psi}/\hat{x}^{1/2}$ and

$$\hat{H} = 2^{1/4}\pi^{1/2}V(1, \hat{\zeta}/\sqrt{2})\exp\{-\hat{\zeta}^2/8\}. \tag{68}$$

This solution is consistent with exponentially small values of T between the dividing streamline and the wall. The thickness y of the transition layer grows like $\sigma^{-1/2}x^{-1/2}$ as $x \to 0+$, consistent with the form (55) emanating from the separation zone, and it also grows (like $\sigma^{-1/2}x^{1/3}$) as $x \to \infty$ where it lies within the shear layer discussed in Section 3.

5. Solution of the separation-zone problem

The numerical solution of (51–54) together with (60) is based on a marching scheme using a modification of the Keller-box method applied recently to a model thermal boundary-layer separation problem [21]. The governing equations are set up as a system of first order partial differential equations:

$$\frac{\partial \theta}{\partial Y} = \Theta, \tag{69}$$

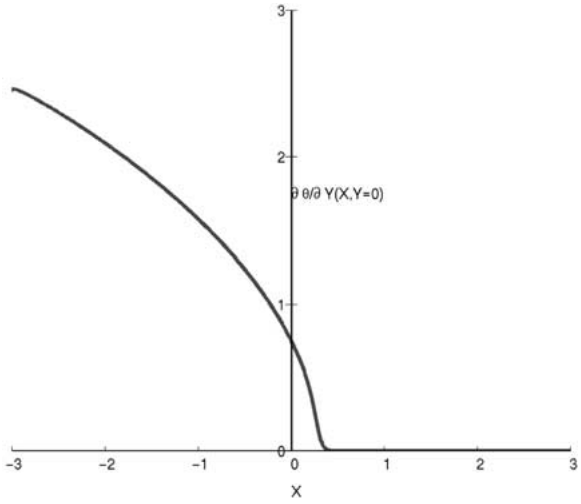

Figure 6. Wall heat transfer in the separation zone obtained from solution of Equations (51–54) together with (60).

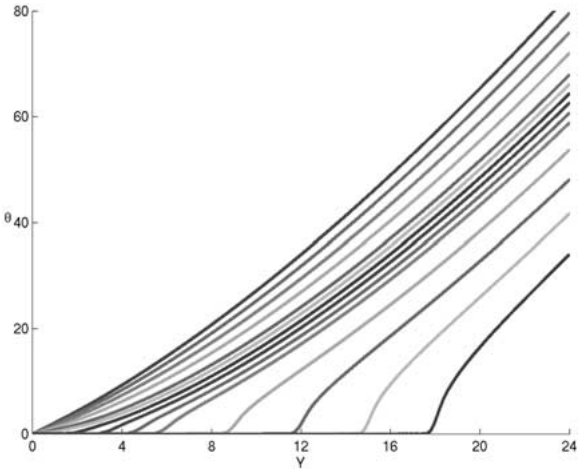

Figure 7. Temperature profiles at $X = -2, -1 \cdot 5, -1, -0{\cdot}5, 0, 0{\cdot}2, 0{\cdot}4, 0{\cdot}6, 0{\cdot}8, 1, 1{\cdot}5, 2, 2{\cdot}5, 3$ (left to right) in the separation zone obtained from solutions of (51–54) together with (60).

$$\frac{\partial \Theta}{\partial Y} = \frac{\partial \Psi}{\partial Y}\frac{\partial \theta}{\partial X} - \frac{\partial \Psi}{\partial X}\Theta, \tag{70}$$

where $\Psi = \frac{1}{6}Y^3 - XY^2$. The computational domain is $[-X_\infty, X_\infty] \times [0, Y_\infty]$ where $X_\infty = 3$ and $Y_\infty = 24$ to accommodate the forward flow above the reverse flow region in $X > 0$. The domain is discretized with step lengths of ΔX and ΔY so that $X_i = X_{i-1} + \Delta X$ and $Y_j = Y_{j-1} + \Delta Y$. At each X_i, the first-order equations are discretized by use of the box scheme.

With the reverse flow region $Y < 4X$ where $\partial\Psi/\partial Y < 0$ denoted by Ω, the modified marching scheme is as follows. On the first forward sweep, solutions for θ, Θ are obtained with $(\partial\Psi/\partial Y)\partial\theta/\partial X = 0$ in Ω as in FLARE; the values of θ and Θ are updated to zero at $X = X_\infty$ on Ω. On the first and subsequent backward sweeps, marching begins at $X = X_\infty - \Delta X$ with θ, Θ known at $X = X_\infty$; if the node is *outside* Ω, the discrete equation

for Θ is replaced by retaining the value of Θ obtained from the previous forward sweep. On the second and subsequent forward sweeps, if the node is *inside* Ω, the discrete equation for Θ is replaced by retaining the value of Θ obtained from the previous backward sweep; the values of θ, Θ are again set to zero at $X = X_\infty$ on Ω, as in the first forward sweep. Since the solution over $X < 0$ is unchanged, forward sweeps are initiated at $X = 0$ on the second and subsequent occasions whilst the backward sweeps are terminated at the same location. Step lengths of $\Delta X = 0{\cdot}00625$ and $\Delta Y = 0{\cdot}0025$ were found to overcome streamwise oscillations attributed to the instability of the box-scheme discretization of convection-diffusion problems [24]. The global L_1 norm for the residuals averaged over the whole computational domain between successive forward-backward sweeps fell below 0·01 in just 20 sweeps with an under-relaxation factor of 0·7 and final results for the wall heat transfer $\Theta(Y = 0)$ and temperature profiles are shown in Figures 6 and 7 respectively.

6. Discussion

The present paper has studied the temperature field of a separating wall jet, with particular emphasis on the large-Prandtl-number limit. New solutions have been found for fixed wall temperature which indicate a sudden reduction in wall heat transfer as the flow separates from the wall. For general values of the Prandtl number σ, the streamwise length scale $\overline{x}$ over which this reduction occurs is of order $R^{-3/14}$ and from the numerical results shown in Figure 2, this scale decreases as σ increases. For small σ, most of the reduction in heat transfer occurs downstream of the separation point, whereas for large σ it occurs almost entirely upstream. From the scale transformations (17) it follows that for the stratified wall jet considered here, this upstream length scale is of order $R^{-3/14}\sigma^{-1/7}$ as $\sigma \to \infty$ although the key adjustment in the temperature field occurs within the separation zone shown in Figure 5, which has a shorter streamwise length scale $R^{-3/14}\sigma^{-10/21}$ and is centred on the point of separation. The detailed structure of the temperature field has been determined in the separation zone, taking full account of the upstream influence in the solution resulting from flow reversal in the jet. This upstream influence is characterized by a non-uniqueness of the solution downstream of the separation point, the form of which is found analytically in Section 3.

The results reported here correspond to solutions for which the temperature of the fluid in the region of weak reverse flow downstream of separation approaches that of the wall, with the adjustment to the ambient temperature being made outside the dividing streamline. It seems likely that a wider class of temperature fields is possible in which the region between the dividing streamline and the wall is convection-dominated corresponding, for example, to non-zero values of k in (35) or, for the large-Prandtl-number limit, non-zero values of K in (60). Initial indications are that such solutions do exist in the latter case, just as they do in a related thermal boundary-layer problem [21] and correspond here to setting $\theta = K(-\Psi/6)^{1/2}$ (instead of zero) in the reverse flow region at the downstream location $X = X_\infty$ in the algorithm described in Section 5. The physical significance of such solutions, however, depends upon an understanding of how the double-deck structure fits into a wider picture of the flow for a particular geometry and this is a much more difficult proposition.

Acknowledgements

The work reported here was partially supported by a grant from the UK Science and Engineering Research Council. The authors are grateful to R. E. Hulse for assistance with the production of Figure 5.

References

1. F. T. Smith and P. W. Duck, Separation of jets or thermal boundary layers from a wall. *Quart. J. Mech. Appl. Math.* 30 (1977) 143–156.
2. I. Flugge-Lotz and T. A. Reyhner, The interaction of a shock wave with a laminar boundary layer. *Int. J. Nonlinear Mech.* 3 (1968) 173–179.
3. A. Liakopoulos, P. A. Blythe, and P. G. Simpkins, Convective flows in tall cavities. In: A. F. Emery (ed.), *Simulation and Numerical Methods in Heat Transfer; ASME Heat Transfer Division* 157 (1990) pp. 81–87.
4. R. P. Clark and N. Toy, Natural convection around the human head. *J. Physiol.* 244 (1975) 283–293.
5. G. A. Feldhamer, S. H. Drickamer, S. H. Vessey, and J. F. Merritt, *Mammalogy: Adaptation, Diversity, and Ecology*. Dubuque: Wm. C. Brown/McGraw-Hill (1999) 563 pp.
6. A. Shkolnik, C. R. Taylor, V. Finch, and A. Borut, Why do bedouins wear black robes in hot deserts? *Nature* 283 (1980) 373–375.
7. A. E. Gill, The boundary layer regime for convection in a rectangular cavity. *J. Fluid Mech.* 26 (1966) 515–553.
8. A. F. Messiter and A. Liñan, The vertical plate in laminar free convection: effects of leading and trailing edges and discontinuous temperatures. *J. Appl. Math. Phys. (ZAMP)* 27 (1976) 633–651.
9. F. T. Smith, A note on a wall jet negotiating a trailing edge. *Quart. J. Mech. Appl. Math.* 31 (1978) 473–479.
10. J. H. Merkin and F. T. Smith, Free convection boundary layers near corners and sharp trailing edges. *J. Appl. Math. Phys. (ZAMP)* 33 (1982) 36–52.
11. J. H. Merkin, Free convection boundary layers over humps and indentations. *Quart. J. Mech. Appl. Math.* 36 (1983) 71–85.
12. K. Gersten, M. Grobel, H. Klick, and M. Merzkirch, Flow separation in laminar natural convection. *Int. J. Heal Fluid Flow* 12 (1991) 331–335.
13. S. Ghosh Moulic and L. S. Yao, Natural convection near a small protrusion on a vertical plate. *Int. J. Heat Mass Transfer* 35 (1992) 2931–2940.
14. M. El Hafi, *Asymptotic Analysis and Model Coupling Applied to Natural Convection Boundary Layers.* PhD thesis. University Paul Sabatier. Toulouse. France (1994).
15. F. J. Higuera, Opposing mixed convection flow in a wall jet over a horizontal plate. *J. Fluid Mech.* 342 (1997) 355–375.
16. J. W. Elder, Laminar free convection in a vertical slot. *J. Fluid Mech.* 23 (1965) 77–98.
17. K. Stewartson and P. G. Williams, Self-induced separation II. *Mathematika* 20 (1973) 98–108.
18. S. Saintlos, J. Mauss, and A. Rigal, Local relaxation method for boundary layer equations with separation. *Int. J. Eng. Sci.* 32 (1994) 409–416.
19. S. Saintlos, M. El Hafi, A. Rigal, and J. Mauss, Numerical solution of boundary layer problem with separation. In: C. Bandle, J. Bemelmans, M. Chipot, J. Saint Jean Paulin and I. Shafrir (eds.), *Calculus of Variations, Applications and Computations, Research Notes in Mathematics* 326 (1995) pp. 215–229.
20. A. K. Aziz, D. A. French, S. Jensen, and R. B. Kellogg, Origins, analysis, numerical analysis, and numerical approximation of a forward-backward parabolic problem. *Math. Model. Num. Anal.* 33 (1999) 895–922.
21. J. T. Ratnanather and P. G. Daniels, Solution of the thermal boundary layer equations in regions of flow reversal. *SIAM J. Appl. Math.* 55 (1995) 192–204.
22. M. Abramowitz and I. A. Stegun, *Handbook of Mathematical Functions* (9th edition). New York: Dover (1972) 1064 pp.
23. M. J. Lighthill, Contributions to the theory of heat transfer through a laminar boundary layer. *Proc. R. Soc. London* A202 (1950) 359–377.
24. D. C. L. Lam, Modal analysis of semidiscrete problems for the diffusion-convection problem. In: R. S. D. Thomas and H. C. Williams (eds.), *Proc. 3rd Manitoba Conf. Num. Math.*, volume IX of *Congressus Numerantium* (1974) pp. 277–286.